Mo-Cu 合金与 1Cr18Ni9Ti 不锈钢真空钎焊接头的组织性能

王 娟， 郑德双， 李亚江
（山东大学 材料液固结构演变与加工教育部重点实验室，济南 250061）

王 娟

摘 要： 采用 Ag-Cu-Ti 钎料，控制钎焊温度为 910 ℃，保温时间为 20 min，可以实现 Mo-Cu 合金与 1Cr18Ni9Ti 不锈钢的真空钎焊，接头抗剪强度为 75 MPa. 采用扫描电镜、能谱分析仪和显微硬度计对 Mo-Cu/1Cr18Ni9Ti 接头组织特征及性能进行分析. 结果表明，钎焊接头靠近 1Cr18Ni9Ti 钢一侧，主要形成 Ag-Cu 共晶组织和少量的 TiC 相；靠近 Mo-Cu 合金一侧，Ag，Cu 元素在合金与钎缝间相向扩散，共晶组织消失，以富铜相为主. 钎缝的显微硬度明显低于 Mo-Cu 合金和 1Cr18Ni9Ti 不锈钢母材，无脆性化合物生成，剪切断口呈现剪切韧窝的形貌特征.

关键词： Mo-Cu 合金；1Cr18Ni9Ti 不锈钢；真空钎焊；组织特征
中图分类号： TG457 **文献标识码：** A **文章编号：** 0253－360X(2013)01－0013－04

0 序 言

高致密度 Mo-Cu 合金具有高导电导热性、低线膨胀系数和良好的高温性能，已用于电子封装和散热材料，尤其在对重量要求较高的便携式设备、航空航天仪器上有很好的应用前景[1-3]. 如将 Mo-Cu 合金与 1Cr18Ni9Ti 不锈钢连接制成复合构件，可充分发挥 Mo-Cu 合金高导电、高导热和 1Cr18Ni9Ti 不锈钢抗氧化、耐腐蚀的性能优点，弥补 Mo-Cu 合金抗高温氧化能力的不足，提高结构件的整体性能.

Mo-Cu 合金与 1Cr18Ni9Ti 不锈钢焊接时，由于两者线膨胀系数和导热能力相差较大，接头处易产生很大的应力，增加裂纹倾向、降低焊缝的力学性能. 并且 Mo-Cu 合金对气体杂质较敏感，接头处易产生气孔，快速冷却时，间隙杂质还会在晶界上形成偏析[4]. Mo-Cu 合金焊接主要采用电子束焊[5]、钨极氩弧焊[6]及活化钎焊[7]等工艺. 研究结果表明，Mo-Cu 合金的焊接在真空环境中进行，可有效抑制氧和氮的有害作用，避免焊接裂纹的产生.

热物理性能差异较大的不同材料焊接时，较多采用固相焊方法[8,9]. 文中采用 Ag-Cu-Ti 钎料对 Mo-Cu 合金与 1Cr18Ni9Ti 不锈钢进行真空钎焊，采用扫描电镜和能谱分析仪研究 Mo-Cu 合金与 1Cr18Ni9Ti 不锈钢钎焊接头的微观组织结构，采用显微硬度计测定接头组织性能，分析接头的断裂特征，为促进 Mo-Cu 合金的应用提供理论基础.

收稿日期： 2011－11－22
基金项目： 国家自然科学基金资助项目(51005135)；山东大学自主创新基金资助项目(2010TS068)

1 试验方法

试验母材为 Mo-Cu 合金和 1Cr18Ni9Ti 不锈钢，板厚为 2.5 mm. Mo-Cu 合金的化学成分(质量分数)为 70% Mo，30% Cu，1Cr18Ni9Ti 不锈钢的化学成分见表 1. Mo-Cu 合金的微观组织形貌见图 1.

表 1 1Cr18Ni9Ti 不锈钢的化学成分(质量分数，%)
Table 1 Chemical compositions of 1Cr18Ni9Ti stainless steel

C	Cr	Ni	Mn	Si	Ti	S	P	Fe
0.10	18.10	8.44	1.82	0.82	0.66	0.03	0.03	余量

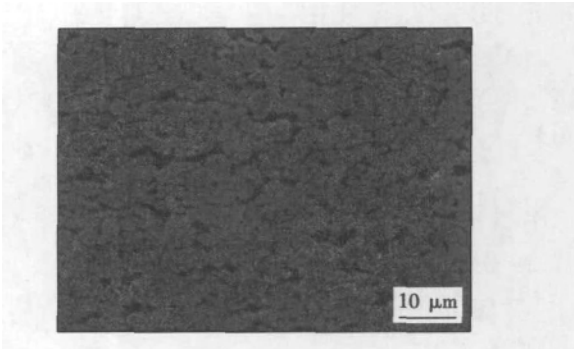

图 1 Mo-Cu 合金的微观组织形貌
Fig. 1 Microstructure of Mo-Cu alloy

焊前清除母材待焊表面的氧化物及油污，采用膏状 Ag-26%Cu-2%Ti 钎料进行真空钎焊，真空度大于 10^{-4} Pa. 钎焊温度为 910 ℃，保温时间为 20 min，焊后冷却至 100 ℃，取出试件.

焊后采用线切割方法对 Mo-Cu/1Cr18Ni9Ti 接头进行取样，磨制抛光后采用王水溶液腐蚀 5 ~ 10 s 制备成金相试样. 采用 CMT 5105 拉伸试验机测定接头的抗剪强度；采用 SHIMADZU 显微硬度计测定接头的显微硬度，载荷为 0.5 N，加载 10 s；采用 1500Nikon AFX-IIA 金相显微镜、QUANTA200 扫描电镜及其附带的 INCAX-SIGHT 能谱分析仪分析接头区的微观组织形貌和断口特征.

2 试验结果与分析

2.1 接头组织特征

图 2 为 Mo-Cu/1Cr18Ni9Ti 接头的微观组织形貌. Ag-Cu-Ti 钎料与 Mo-Cu 合金及 1Cr18Ni9Ti 不锈钢具有良好的润湿性，钎缝与两侧母材结合紧密，接头没有裂纹、显微孔洞等缺陷存在，如图 2a 所示.

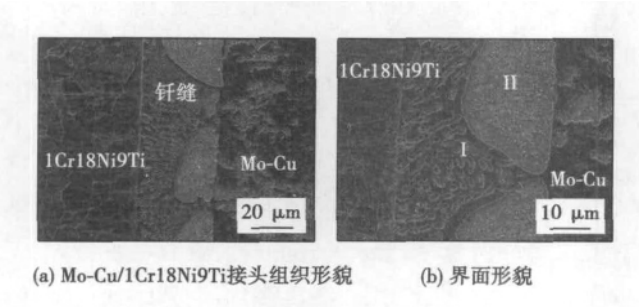

图 2 Mo-Cu/1Cr18Ni9Ti 接头的微观组织形貌

Fig. 2 Microstructure of Mo-Cu/1Cr18Ni9Ti joint

获得的钎缝组织主要包括靠近 1Cr18Ni9Ti 一侧的共晶组织(I)和靠近 Mo-Cu 合金一侧的块状组织(II)，如图 2b 所示. 图 3 为钎缝与 Mo-Cu 合金及 1Cr18Ni9Ti 钢两侧界面的扫描电镜形貌. 表 2 为采用能谱分析仪测得的图 3 中 A-F 各点化学成分.

A 点成分表明是 1Cr18Ni9Ti 不锈钢母材. 在钎缝与 1Cr18Ni9Ti 不锈钢结合界面上有少量的白色点状组织生成(B 点)，成分分析(表 2)表明，形成的是 TiC. 这是由于 Ag-Cu-Ti 钎料中的 Ti 元素在钎焊时向钢侧扩散，与碳发生反应形成的. 钎缝靠近 1Cr18Ni9Ti 钢侧主要生成的是 Ag-Cu 共晶组织，如图 3b 中的 C 点和 D 点. C 点含 3.7% Ag，96.0% Cu 和 0.2% Ti，D 点含 89.6% Ag，10.3% Cu 和 0.1% Ti. 根据 Ag-Cu 二元相图，C 点为共晶成分的富铜固溶体；D 点为共晶成分的富银固溶体.

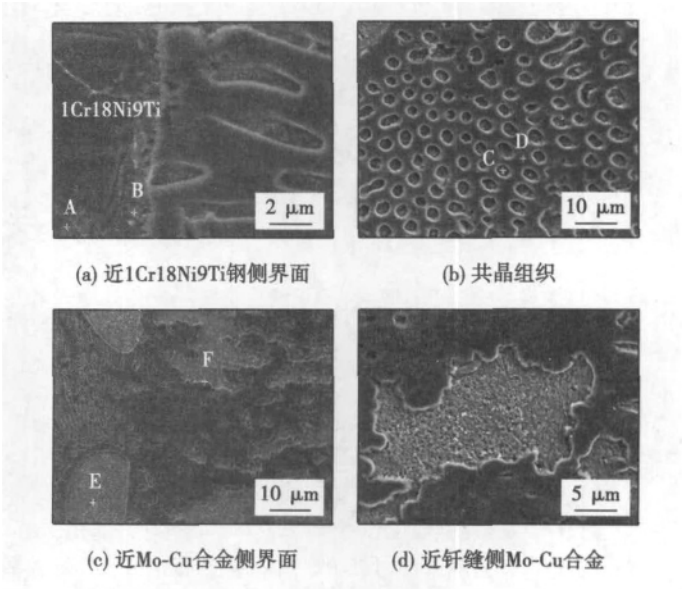

图 3 钎缝与母材界面的微观形貌

Fig. 3 Interfacial characteristics of Mo-Cu/1Cr18Ni9Ti joint

表 2 Mo-Cu/1Cr18Ni9Ti 接头各点的成分分析(质量分数，%)

Table 2 Compositions of points in Mo-Cu/1Cr18Ni9Ti joint

位置	Ag	Cu	Ti	C	Fe	Cr	Ni	Mo	形成的相
A	—	—	0.8	0.1	73.0	17.9	8.2	—	1Cr18Ni9Ti 母材
B	1.5	4.5	46.2	41.2	1.6	3.8	1.2	—	TiC
C	3.7	96.0	0.2	—	0.1	—	—	—	富铜相固溶体
D	89.6	10.3	0.1	—	—	—	—	—	富银相固溶体
E	16.1	83.8	0.1	—	—	—	—	—	铜
F	32.3	12.9	0.2	—	—	—	—	54.6	Mo-Cu(Ag)

图 3c 为钎缝与 Mo-Cu 合金界面的微观组织形貌. 靠近 Mo-Cu 合金侧的钎缝没有共晶组织生成，主要是由于钎焊过程中，Mo-Cu 合金中的铜向钎缝中心扩散，同时从合金中钼颗粒周围明显分布富含 Ag 元素的白色相，断定 Ag 元素则从钎料向合金中扩散，两种元素的相向扩散导致靠近合金侧共晶组织消失，出现富铜相，如图 3b 中的 E 点所示，铜含量为 83.8%.

从 Mo-Cu/1Cr18Ni9Ti 接头微观组织形貌及成分分布可见，钎缝与 Mo-Cu 合金间平缓过渡，没有类似 1Cr18Ni9Ti 钢侧的明显界面，主要是因为 Cu，Mo，Ag 等元素之间发生固溶反应，而不是化学反应. 图 3c 中 F 点成分主要含 54.6% Mo，32.3% Ag 和 12.9% Cu. 在接头靠近 Mo-Cu 合金侧，钼与其它金属元素无明显互溶，而是独立存在；因此灰色基体是钼，白色相银环绕在钼颗粒周围，如图 3d 所示.

2.2 显微硬度

为分析 Mo-Cu/1Cr18Ni9Ti 接头组织对性能的

影响,采用显微硬度计对 1Cr18Ni9Ti、钎缝及 Mo-Cu 合金的显微硬度进行测定,测试位置及显微硬度分布如图 4 所示.

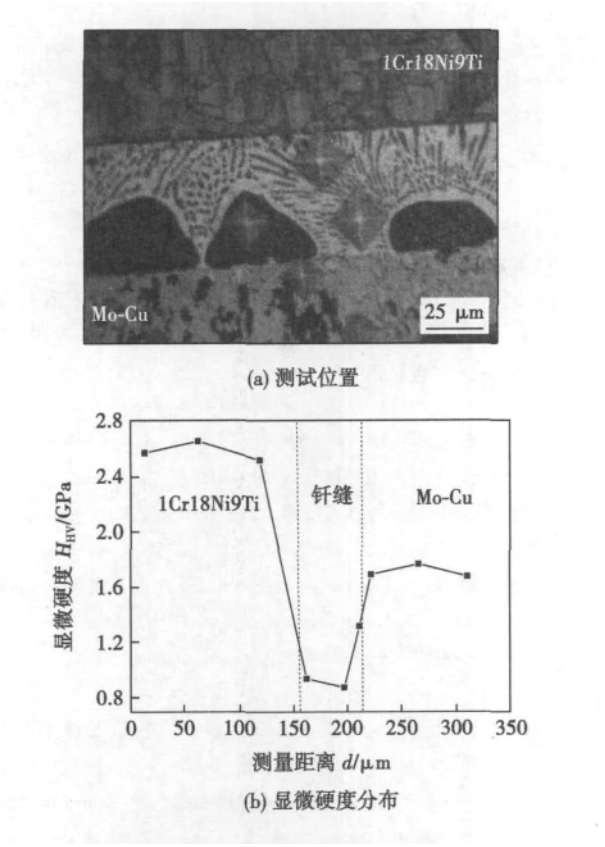

图 4　Mo-Cu/1Cr18Ni9Ti 接头的显微硬度

Fig. 4　Microhardness of Mo-Cu/1Cr18Ni9Ti joint

可以看出,1Cr18Ni9Ti 不锈钢一侧平均显微硬度为 2.6 GPa,Mo-Cu 合金侧的平均显微硬度为 1.8 GPa,而钎缝中心显微硬度较低,平均只有 1.2 GPa,这主要与钎缝中心形成的 Ag-Cu 共晶组织有关,如图 4a 所示. 虽然靠近 Mo-Cu 合金一侧的块状富铜相的显微硬度值大于 Ag-Cu 共晶组织的显微硬度,但明显小于两侧 Mo-Cu 合金和 1Cr18Ni9Ti 的显微硬度. 因此采用 Ag-Cu-Ti 钎料,控制温度为 910 ℃,保温时间为 20 min 时,钎缝没有形成脆性较大的金属间化合物,有利于保证接头的组织性能.

2.3　断口形貌

图 5 为 Mo-Cu/1Cr18Ni9Ti 接头抗剪断口形貌及成分分布. 试验用 1Cr18Ni9Ti 钢的抗剪强度为 220 MPa,Mo-Cu 合金的抗剪强度为 280 MPa. Mo-Cu/1Cr18Ni9Ti 搭接接头的平均抗剪强度为 75 MPa,约为 1Cr18Ni9Ti 抗剪强度的 34%,Mo-Cu 合金抗剪强度的 27%. 接头剪切断口形貌如图 5a,c 所示. 可见断口呈现明显的剪切韧窝形貌特征,因此获得的 Mo-Cu/1Cr18Ni9Ti 钎焊接头具有塑性断裂特征.

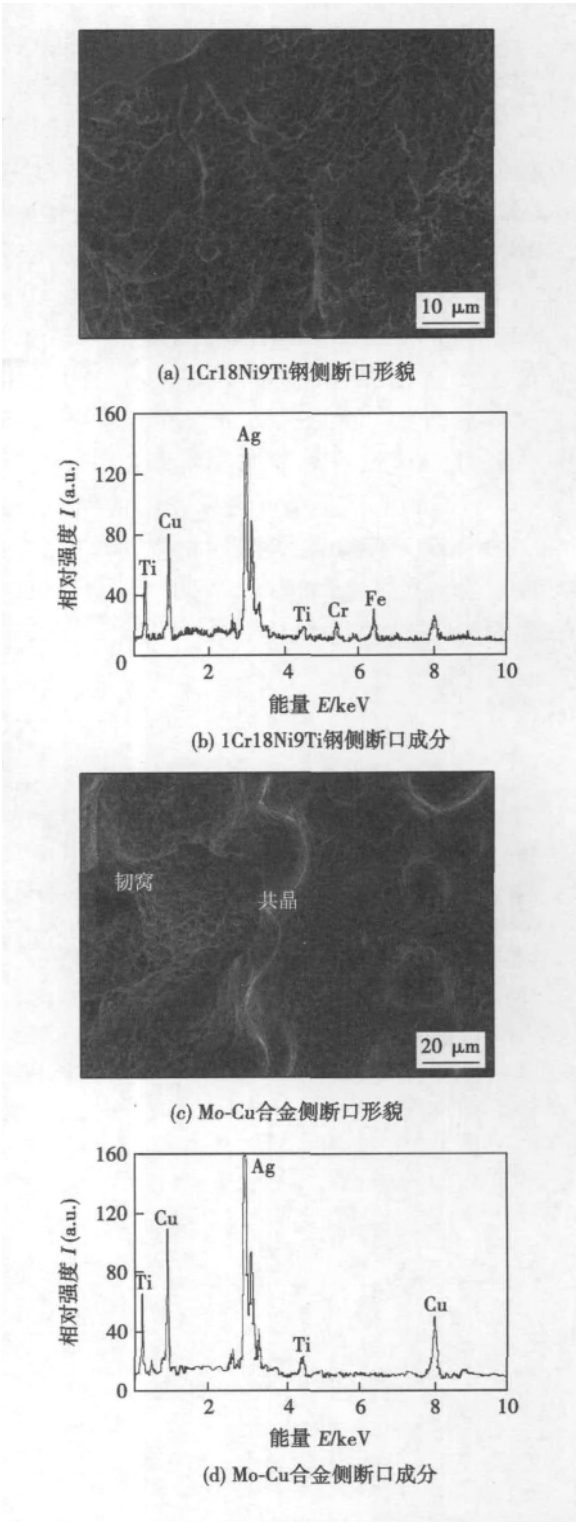

图 5　Mo-Cu/1Cr18Ni9Ti 接头剪切断口形貌及成分分布

Fig. 5　Shear fracture morphology and element distribution in Mo-Cu/1Cr18Ni9Ti joint

采用能谱分析分别对 1Cr18Ni9Ti 钢和 Mo-Cu 合金的剪切面进行成分分析,见图 5b, d. 1Cr18Ni9Ti 侧主要存在银、铜、钛、铁和铬,Mo-Cu 合金侧主要存在银、铜和钛,无钼存在. 因此接头断裂

主要发生在钎缝靠近 1Cr18Ni9Ti 侧界面处. 这主要是由于在界面附近形成的 Ag-Cu 共晶组织所致.

3 结 论

(1) 采用 Ag-Cu-Ti 钎料,控制钎焊温度为 910 ℃,保温时间为 20 min 时,可以实现 Mo-Cu 合金与 1Cr18Ni9Ti 不锈钢的真空钎焊,接头抗剪强度达 75 MPa.

(2) Mo-Cu/1Cr18Ni9Ti 接头靠近 1Cr18Ni9Ti 钢一侧,主要形成 Ag-Cu 共晶组织和少量的 TiC 相;靠近 Mo-Cu 合金一侧,Ag,Cu 元素在合金与钎缝间相向扩散,共晶组织消失,以富铜相为主.

(3) 钎缝中心的显微硬度低于两侧 Mo-Cu 合金和 1Cr18Ni9Ti 不锈钢,无脆性化合物生成;接头剪切断裂发生在钎缝靠近 1Cr18Ni9Ti 结合界面处,断口呈现剪切塑性断裂特征.

参考文献:

[1] Tikhii G A, Kachalin N L, Belova V P, *et al*. Study of a Mo-Cu pseudo-alloy obtained from mechanically activated charge [J]. Metal Science and Heat Treatment, 2007, 49(9): 448 - 452.

[2] Kiselev S P. Compaction of a mixture of copper and molybdenum nanopowders modeled by the molecular dynamics method [J]. Journal of Applied Mechanics and Technical Physics, 2008, 49(5): 712 - 722.

[3] 白培康, 刘 斌, 胡胜亮. Mo/Cu 复合材料构件激光快速成型工艺 [J]. 中国有色金属学报, 2008, 18(6): 1094 - 1099.
Bai Peikang, Liu Bin, Hu Shengliang. Laser rapid prototyping process of Mo/Cu composites part [J]. The Chinese Journal of Nonferrous Metals, 2008, 18(6): 1094 - 1099.

[4] Cockeram B V, Ohriner E K, Byun T S, *et al*. Weldable ductile molybdenum alloy development [J]. Journal of Nuclear Materials, 2008, 382(2): 229 - 241.

[5] Matsuds F, Ushio M, Nakata K. Weldability of molybdenum and its alloy sheet [J]. Transactions of JWRI, 1990, 19(1): 69 - 78.

[6] 王 娟, 李亚江, 郑德双, 等. 填丝 TIG 焊接 Mo-Cu 合金与 18-8 不锈钢接头的微观组织 [J]. 焊接学报, 2011, 32(12): 77 - 80.
Wang Juan, Li Yajiang, Zheng Deshuang, *et al*. Microstructure of Mo-Cu alloy and 18-8 stainless steel joint by TIG with filler metal [J]. Transactions of the China Welding Institution, 2011, 32(12): 77 - 80.

[7] Singh M, Asthana R. Characterization of brazed joints of C/C composite to Cu-clad-Molybdenum [J]. Composites Science and Technology, 2008, 68(14): 3010 - 3019.

[8] 王全兆, 刘 越, 张玉政, 等. TiC/NiCr 金属陶瓷与 1Cr13 不锈钢的真空钎焊 [J]. 焊接学报, 2006, 27(8): 43 - 46.
Wang Quanzhao, Liu Yue, Zhang Yuzheng, *et al*. Vacuum brazing between TiC/NiCr cermets and 1Cr13 stainless steel [J]. Transactions of the China Welding Institution, 2006, 27(8): 43 - 46.

[9] 邹贵生, 闫剑锋, 母凤文, 等. 微连接和纳连接的研究新进展 [J]. 焊接学报, 2011, 32(4): 107 - 112.
Zou Guisheng, Yan Jianfeng, Mu Fengwen, *et al*. Recent progress in microjoining and nanojoining [J]. Transactions of the China Welding Institution, 2011, 32(4): 107 - 112.

作者简介: 王 娟,女,1977 年出生,博士,副教授. 主要从事先进材料及特种焊接技术方面的研究. 发表论文 30 余篇. Email: jwang@sdu.edu.cn

MAIN TOPICS, ABSTRACTS & KEY WORDS

Analysis on hydrogen induced peeling behavior in fusion zone between base metal and austenitic stainless steel overlayer in hydro-processing reactors DU Bing[1], JIA Yuli[1], RAO Qingpeng[2] (1. Harbin Welding Institute, China Academy of Machinery Science and Technology, Harbin 150080, China; 2. School of Material Science and Engineering, Dalian Jiaotong University, Dalian 116028, China). pp 1 - 3

Abstract: Hydrogen induced peeling in the fusion zone between base metal and austenitic stainless steel overlayer is the main problem of hydro-processing reactors in practical operation. Focused on the widely applied 309L + 347L austenitic stainless steel overlaying process, the simulation experiments in the high temperature autoclave indicated the peeling crack germinated at the pure austenitic grain boundaries close to the hardening zone (the microstructure in this region is very complex as a consequence of carbon migration during PWHT(post weld heat treatment) and incomplete mixing of melted base metal and stainless steel fillers) of fusion zone between base metal and austenitic stainless steel overlayers and propagated along the austenitic grain boundaries. Based on the experimental investigation, it is the embrittlement of austenitic grain boundaries induced by the hydrogen accumulation and the high residual shearing stress at the overlay interface that cause the hydrogen induced peeling. The experimental results showed that smaller heat input for 309L overlaying, appropriate PWHT and smaller cooling rate of hydro-processing reactors are all helpful measurements to prevent hydrogen induced peeling.

Key words: stainless steel overlaying; fusion zone; hydrogen induced peeling; hydro-processing reactor

Numerical simulation of longitudinal plastic strain field in thin-plate weldment of aluminum alloy LI Jun[1,2], ZHANG Wenfeng[2], ZHENG Yansong[1], LOU Haoyue[2] (1. State Key Laboratory of Advanced Welding and Joining, Harbin Institute of Technology, Harbin 150001, China; 2. Zhejiang Yinlun Machinery Co., Ltd., Tiantai 317200, China). pp 4 - 8

Abstract: The welding longitudinal plastic strain field was simulated by elastic-plastic FEM analysis software. The simulation results showed that, for butt weldment made of 2A12-T4 aluminum alloy thin plates with 200 mm in length, 100 mm in width and 2 mm in thickness, only longitudinal tensile plastic strain exists in the weld metal after welding, while in the zone close to the weld, not only longitudinal compressive plastic strain but also longitudinal tensile plastic strain exist. The distribution of residual longitudinal plastic strain along the welding seam is not uniform, especially complex at the zone near the ends of weld seam. The uneven distribution of longitudinal plastic strain in the zone close to the weld can be attributed to the combination of the variation of temperature field with the difference of load-carrying state of the metal beside the heating source during welding.

Key words: welding; aluminum alloy; plastic strain; numerical simulation

Microstructure, friction and wear properties of Ni-based alloy coating on Monel alloy substrate by laser cladding ZHANG Song[1], ZHOU Lei[1], HAO Yuxi[1], ZHANG Chunhua[1], WANG Dongsheng[2], WANG Maocai[2] (1. School of Materials Science and Engineering, Shenyang University of Technology, Shenyang 110870, China; 2. The Shenyang Jinyan Laser Manufacturing Technology Development Co., Ltd., Shenyang 110870, China). pp 9 - 12

Abstract: The Ni-based alloy modified coating was fabricated on Monel 400 alloy by laser cladding technology. The characteristics of microstructure and compositions of the laser deposited layer were studied by scanning electron microscopy (SEM), energy dispersive spectroscopy (EDS) and X-ray diffraction (XRD). The microhardness, friction and wear properties were analyzed and tested by microhardness tester and pin-dish abrasion tester. The results show that the Ni-based alloys modified layer was mainly composed of γ-Ni solid solution, multi-eutectic and some primary precipitation phase. The Ni-based alloys modified layer with excellent performance can be obtained with the optimal laser processing parameter. The microhardness of the laser modified layer is 7 times as big as that of the substrate. The friction coefficient of the laser modified layer was significantly reduced and the relative wear resistance increased by 8.6 times.

Key words: laser cladding; Monel alloy; Ni-based alloys; microstructure; friction and wear

Microstructure characteristics of vacuum brazed joint for Mo-Cu alloy with 1Cr18Ni9Ti stainless steel WANG Juan, ZHENG Deshuang, LI Yajiang (Key Laboratory for Liquid-Solid Structural Evolution & Processing of Materials, Ministry of Education, Shandong University, Jinan 250061, China). pp 13 - 16

Abstract: Mo-Cu alloy and 1Cr18Ni9Ti stainless steel were joined by vacuum brazing with Ag-Cu-Ti active filler metal at 910 ℃ for 20 min and a Mo-Cu/1Cr18Ni9Ti joint with a shear strength of 75 MPa was obtained. The microstructure and performance of Mo-Cu/1Cr18Ni9Ti joint were investigated by scanning electron microscope (SEM), energy dispersive spectrometer (EDS) and microhardness test. The results indicated that Ag-Cu eutectic and Cu-rich phase were produced in the brazed joint. There were few of TiC phases near the side of 1Cr18Ni9Ti stainless steel in the joint. The microhardness of brazed seam was lower than that of Mo-Cu alloy and 1Cr18Ni9Ti stainless steel. There are no brittle compounds formed in the Mo-Cu/1Cr18Ni9Ti joint. The shear fracture appearance shows shear dimple feature.

Key words: Mo-Cu alloy; 1Cr18Ni9Ti stainless steel; vacuum brazing; microstructure

Behaviors of element density distribution and melting metal flow in CO_2 laser-MAG hybrid welding LIU Shuangyu, ZONG Shishuai, LIU Fengde, ZHANG Hong (College of Mechanical and Electric Engineering, Changchun University of Sci-